Materials Research Express

PAPER

Prediction and validation of residual stresses generated during laser metal deposition of *γ* titanium aluminide thin wall structures

Materials Research Express

PAPER

Prediction and validation of residual stresses generated during laser metal deposition of γ titanium aluminide thin wall structures

RECEIVED
7 April 2019

REVISED
7 July 2019

ACCEPTED FOR PUBLICATION
6 August 2019

PUBLISHED
21 August 2019

Mallikarjuna Balichakra[1], **Srikanth Bontha**[1,4], **Prasad Krishna**[1] and **Vamsi Krishna Balla**[2,3,4]

[1] Additive Manufacturing Laboratory, Department of Mechanical Engineering, National Institute of Technology Karnataka, Surathkal, Mangaluru-575 025, India
[2] Bioceramics and Coatings Division, CSIR-Central Glass and Ceramic Research Institute, 196 Raja S C Mullick Road, Kolkata-700 032, India
[3] Material Innovation Guild, Department of Mechanical Engineering, University of Louisville, Louisville, KY 40208, United States of America
[4] Authors to whom any correspondence should be addressed.

E-mail: srikanth.bonth@nitk.edu.in **and** vamsiballa@cgcri.res.in

Keywords: residual stresses, laser metal deposition, laser engineered net shaping, γ-TiAl, 3D transient thermomechanical modeling, thin-wall structures, temperature gradients

Abstract

The focus of the current work is to predict and validate residual stresses developed during Laser Metal Deposition (LMD) of Gamma Titanium Aluminide (γ-TiAl) alloy by using a combination of numerical modeling and experimental methods. Laser Engineered Net Shaping (LENS), which is one of the commercially available LMD techniques, was used to fabricate γ-TiAl alloy thin wall structures at various processing conditions. These deposits are expected to develop residual stresses due to the rapid heating and cooling cycles involved in the LMD process. 3D transient thermomechanical finite element analysis was used to simulate the LMD process. Thermal gradients and residual stresses were predicted from the thermomechanical models. It was found that the magnitude of thermal gradients increases with the addition of each deposited layer. Tensile residual stresses were observed at the edges of the thin-wall, while compressive residual stresses were observed at the center of the wall as well as in regions away from the edges. Residual stresses in the deposited samples were also measured using the x-ray diffraction technique. Reasonable agreement was observed between the predicted and measured values of residual stresses.

1. Introduction

Gamma-titanium aluminides (γ-TiAl) are gaining attention in recent years because of their attractive properties such as low density, high strength, good corrosion and oxidation resistance. They are under consideration for applications in aerospace, automotive, and powerplant sectors [1, 2]. γ-TiAl is an intermetallic and hence possesses low ductility and fracture toughness. Therefore, it is difficult to process γ-TiAl at room temperature. Also, a number of post-processing operations are required to achieve uniform microstructure and desired properties which increases the cost of fabrication [3]. Therefore, researchers are trying to find new routes for processing γ-TiAl alloys. Metal additive manufacturing techniques such as powder bed fusion processes and directed energy deposition processes are currently under consideration for fabrication of γ-TiAl components. Zhang *et al* [4] optimized the Laser Engineered Net Shaping (LENS) process parameters to yield quality γ-TiAl samples. The rapid heating and cooling rates associated with the LMD process leads to the development of residual stresses which could result in cracking of samples during deposition. Balla *et al* [5] deposited γ-TiAl samples at different laser energy density conditions and reported that defect free γ-TiAl components were produced only when the laser energy density was between 40 to 50 J mm^{-2}. At all other laser energy densities ($<$40 J mm^{-2} and $>$50 J mm^{-2}) deposition of defective samples due to thermal stresses and poor melting was reported. The high thermal stresses developed during deposition affect microstructure, fatigue life, corrosion resistance and dimensional stability of components [6, 7]. Hence, an understanding of the origin and

development of residual stresses is necessary for producing defect-free γ-TiAl components using LMD techniques.

Several researchers used a combination of numerical modelling and experimental methods to optimize process conditions, and investigated the evolution of residual stresses during LMD of various materials [8–14]. Rangaswamy *et al* [8] reported the measurement of residual stresses in laser-deposited SS 316 and IN 718 rectangular and square samples using neutron diffraction and contour methods. They reported tensile stresses at the edges and compressive stresses at the center of the samples. Moat *et al* [9] built Waspaloy samples using laser deposition technique, and measured residual stresses using neutron diffraction technique. Their study reports tensile stresses at the top surface and compressive stresses closer to the substrate. Sheng *et al* [11] carried out a three-dimensional transient thermomechanical analysis of LMD process during deposition of Ni60A using ANSYS software. Melt pool temperatures and stresses were predicted. It was reported that the predicted melt pool temperatures showed good agreement with experimentally (CCD colorimeter) measured temperatures. Wang *et al* [14] studied the effect of process parameters on residual stress build-up in LENS deposited AISI 410 stainless steel samples. They measured residual stresses using the neutron diffraction method and also carried out a thermomechanical analysis of thin-wall geometries to predict residual stresses. A good agreement between FEM and neutron diffraction results of residual stresses was reported. Pratt *et al* [10] studied the residual stress development in LENS deposited AISI 410 thin plates, both numerically and experimentally. They reported a strong influence of laser power on the development of residual stresses while the effect of laser velocity is minimal. Moat *et al* [12] used the laser deposition technique to fabricate Waspaloy bulky 3D geometries. They measured the residual stresses in these components using neutron diffraction and contour methods. The effect of thermal gradients on residual stress is relatively lower in bulky 3D geometries when compared to thin-wall specimens. Vogel *et al* [13] reported that residual stresses decrease with an increase in the height of SS 316L thin-walls fabricated using laser metal deposition process. It was also reported that stresses and strains are induced in the deposited components due to large thermal gradients. From the literature review, it can be seen that development of residual stresses during laser metal deposition of few materials such as AISI 410, SS316, Ti-6Al-4V, IN718, Ni60A, etc, have been studied by researchers, either using numerical modeling or experimental techniques or both. However, at this time of reporting, there exists no work in the literature on the development of residual stresses in laser metal deposited γ-TiAl.

To this end, the focus of the present work is to understand the influence of process parameters on the state and magnitude of residual stress distribution using a combination of both numerical modeling and experimental approaches. 3D transient thermomechanical finite element analysis was used to simulate LENS deposition of γ-TiAl alloy samples using the commercially available finite element software ANSYS. The developed thermomechanical models were used to understand the influence of process parameters which include laser power and travel speed on melt pool geometry, thermal gradients and residual stresses developed during the LENS process. Samples were then deposited using the LENS process at the same process parameters used in numerical modeling. X-ray diffraction technique was then used to measure the residual stresses at several points along both longitudinal and build directions of the thin wall structures fabricated using the LENS process. Finally, thermomechanical model predictions of residual stresses were compared with residual stresses measured using the x-ray diffraction method.

2. 3D transient thermomechanical finite element analysis

A three-dimensional transient thermomechanical finite element analysis was performed using the commercial software package ANSYS. Melt pool contours, temperature distribution, and residual stresses were predicted from the developed FE models. Temperature dependent material properties such as density, specific heat, thermal conductivity, coefficient of thermal expansion, Young's modulus, Poisson's ratio, and yield strength were given as input to these models, and these property data have been taken from the literature [15–17]. The governing equations used for thermomechanical analysis were also referred to from the existing literature [18–20].

The finite element (FE) models consist of 10 layers representing a total build height of 2.5 mm, as shown in figure 1. Each layer is subdivided into two rows along the height. In each layer, a block of dimensions $0.5 \times 0.5 \times 0.25\,\text{mm}^3$ consisting of 32 elements is activated based on the time interval and movement of laser heat source. The laser beam is approximated as a heat source with a Gaussian distribution, and heat flux was applied on the top surface of the elements. The entire FE model consists of 19,440 elements and 23,635 nodes. After the completion of the numerical simulation, magnitude and distribution of stresses were extracted from the numerical models.

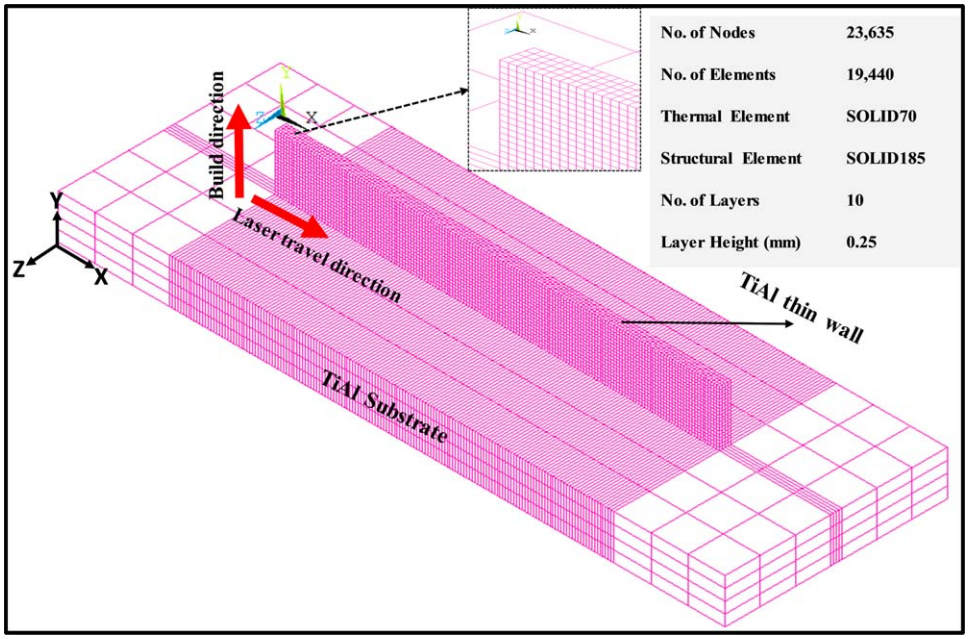

Figure 1. Finite element model of thin wall structure built on a substrate.

Table 1. Process parameters used for depositing thin-wall samples using LENS process.

Sample number	Power (W)	Travel speed (mm s^{-1})	Layer height (mm)	Powder feed rate (g min^{-1})
1	200	8		2.9–3.3
2	200	10	0.25	3.3–3.66
3	200	12		4.0–4.40
4	250	8		2.9–3.3
5	250	10	0.25	3.3–3.66
6	250	12		4.0–4.40
7	300	8		2.9–3.3
8	300	10	0.25	3.3–3.66
9	300	12		4.0–4.40

3. Experimental methodology

3.1. Fabrication of samples by the LENS process

The material used in this study was γ-TiAl alloy powder (Arcam AB, Sweden) with a particle size ranging between 45–150 μm. This γ-TiAl alloy is an intermetallic alloy consisting of Ti, Al, Cr, Nb elements with a composition (at%) of 48, 48, 2, 2, respectively.

Thin wall samples were deposited using LENS machine equipped with a 500 W continuous wave ytterbium-doped fiber laser. The dimensions of the thin-walls are: length: 15 mm, height: 20 mm and thickness: 1.5 mm. These thin walls were built on a γ-TiAl substrate (length: 20 mm, width: 20 mm wide and thickness: 4 mm) using unidirectional scan strategy. Process parameters used for depositing thin-wall samples are presented in table 1. A representative γ-TiAl thin-wall sample fabricated using the LENS process is shown in figure 2(a).

3.2. Experimental measurement of residual stresses

X-ray diffraction (XRD) technique (PROTO iXRD equipped with Cu-Kα radiation, $\lambda = 1.5418$ A°) was used for residual stress measurement. The measurement conditions include 3 mm collimator (Aperture), 25 kV voltage, 4 mA target current, 14 min exposure time, and a scan angle of 142° (2θ). The strain was measured using XRD technique. Finally, stress was determined by substituting slope of the plot 2θ versus $\sin^2\psi$ based on equation (1) [21].

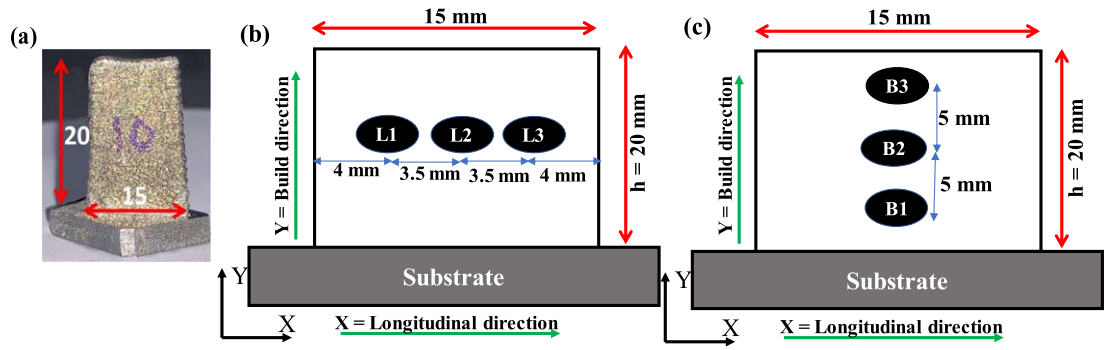

Figure 2. (a) Typical γ-TiAl thin wall deposited on a substrate (b) location of residual stress measurements along longitudinal and (c) build directions.

$$\sigma = -\frac{E}{2(1+\mu)}.\cot\theta_0.\frac{\pi}{180}.\frac{\delta 2\theta}{\delta \sin^2\Psi} \quad (1)$$

Where σ is the stress, E is Young's modulus (260 GPa), μ is Poisson's ratio (0.22), θ_0 and ψ are the diffraction angle corresponding to the stress-free lattice spacing (d_0) and the angle between the diffraction vector to the normal of the surface.

The state and magnitude of residual stress distribution were investigated for all the test samples. A total of six points were considered along the longitudinal and build directions. Figures 1(b) and (c) show the residual stress measurement locations.

4. Results and discussion

LENS deposition of materials involves several reheating and cooling cycles during layer-by-layer deposition. The process results in rapid cooling rates and high thermal gradients which often result in significant thermal stresses leading to warpage. Further, under some conditions, the parts can develop cracks during or immediately after deposition [5]. Therefore, understanding the effect of process parameters on the magnitude and distribution of residual stresses is critical both for manufacturing defect free parts as well as to minimize stress induced warpage. This understanding is even more important for an intermetallic such as γ-TiAl, which is the material under consideration in this study.

4.1. 3D transient thermomechanical finite element analysis results

4.1.1. Melt pool size at different locations

In this section, temperatures and melt pool dimensions were extracted from the finite element models, during deposition of the last layer, both at the centre and also at the free edge of the wall. Temperatures and melt pool contours predicted for P = 200 W, V = 8 mm s^{-1} are shown in figure 3. As illustrated in figure 1, for a single layer the scan path of the laser beam starts at left edge and ends at the right free edge of the wall. An increase in both melt pool dimensions and temperatures were observed as the laser beam approaches the free edges of the wall due to the decreased area available for the conduction of heat. An observation of figures 3(a) and (b) reveals that the maximum temperature at the free edge temperature (3104 °C) is higher compared to that at the center of the wall (2643 °C). The melt pool depth at the center (MPD_c) was 0.3125 mm (figure (c)) whereas it was 0.7625 mm at the free edge (MPD_e) (figure (d)). The thermal gradients at the free edge are higher in magnitude when compared to that at the centre of the wall. This is due to the higher temperatures at the free edge. Further, the temperatures within the melt pool increase as the laser power is increased.

4.1.2. Thermal gradients

The influence of laser power and travel speed on thermal gradients is shown in figures 4(a) and (b). Here, the gradients were extracted along the build direction at the centre of each layer of the thin-wall. Figure 4(a) shows the gradients at different laser powers and at constant travel speed (V = 10 mm s^{-1}). The magnitude of thermal gradient increases from the first layer to the last layer. Lower thermal gradients in the bottom layers can be attributed to rapid heat extraction by the substrate, which acts as a heat sink and conducts the heat away from the melt pool. However, as the number of layers increase the effect of substrate diminishes and therefore thermal gradients increase. Sammons *et al* [22] reported a similar trend of thermal gradients along the build direction.

Further, thermal gradients were found to increase as the laser power increases from 200 W to 300 W. Thermal gradients are the lowest for P = 200 W, V = 10 mm s^{-1} and the highest for the P = 300 W,

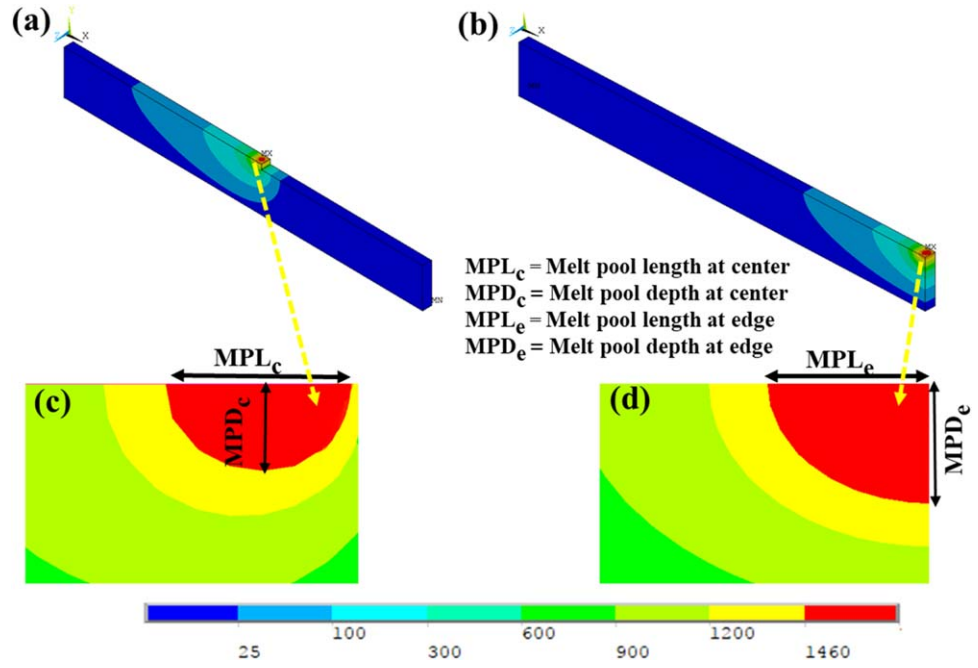

Figure 3. Temperature contours (a), (b) and melt pool size (c), (d) as a function of laser beam location on the thin wall during deposition of the last layer with P = 200 W, V = 8 mm s^{-1}.

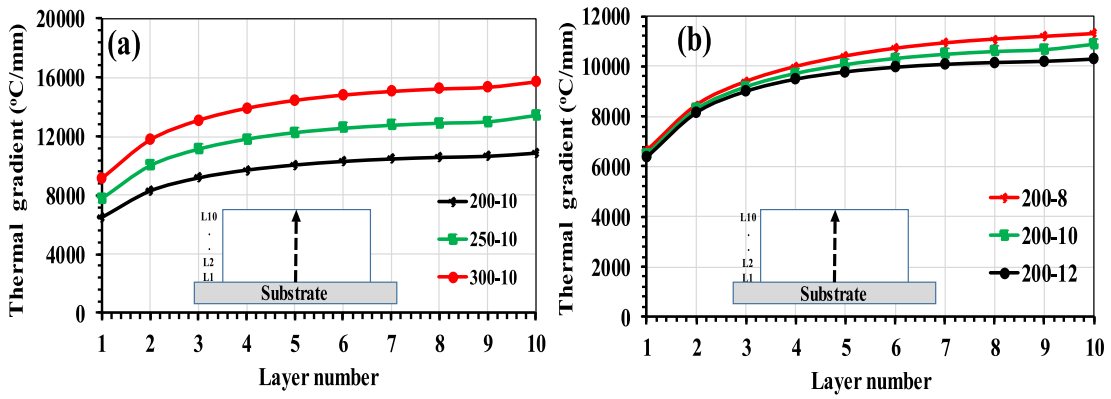

Figure 4. Variation of thermal gradients in different layers during thin wall deposition (a) influence of laser power (b) influence of travel speed.

V = 10 mm s^{-1} conditions, respectively. Figure 4(b) depicts the gradients for various travel speeds at constant power (P = 200 W). The trends in variation of thermal gradients with travel speed are analogous to that reported for variation in laser power. Table 2 presents the thermal gradients in the first and last layer of deposition for all the simulated cases.

4.1.3. Influence of laser power and travel speed on magnitude and distribution of residual stresses

Figures 5(a)–(f) show the stress distribution contours in the thin-wall after cooling to room temperature. Figures 5(a)–(c) were plotted for different laser powers (P = 200, 250, and 300 Watts) at a constant travel speed V = 10 mm s^{-1}. In all cases, tensile stresses were present both at the edges as well as at the top surface of the wall. This is due to expansion and contraction. Whereas, compressive stresses were present in the inner regions of the thin-wall. Further, the magnitude of residual stress increases marginally with an increase in the laser power from 200 to 300 W at a constant travel speed. This is due to the increase in thermal gradients with increase in power (figure 4(a)). Although stress distribution may appear symmetric in the contour plots, a close observation shows peak tensile stresses at the right edge of the wall. This can be attributed to the scanning path where the laser traverses from the left to the right edge. If magnitude of tensile stress in the thin wall exceeds the yield strength of the γ-TiAl then cracking or delamination can occur.

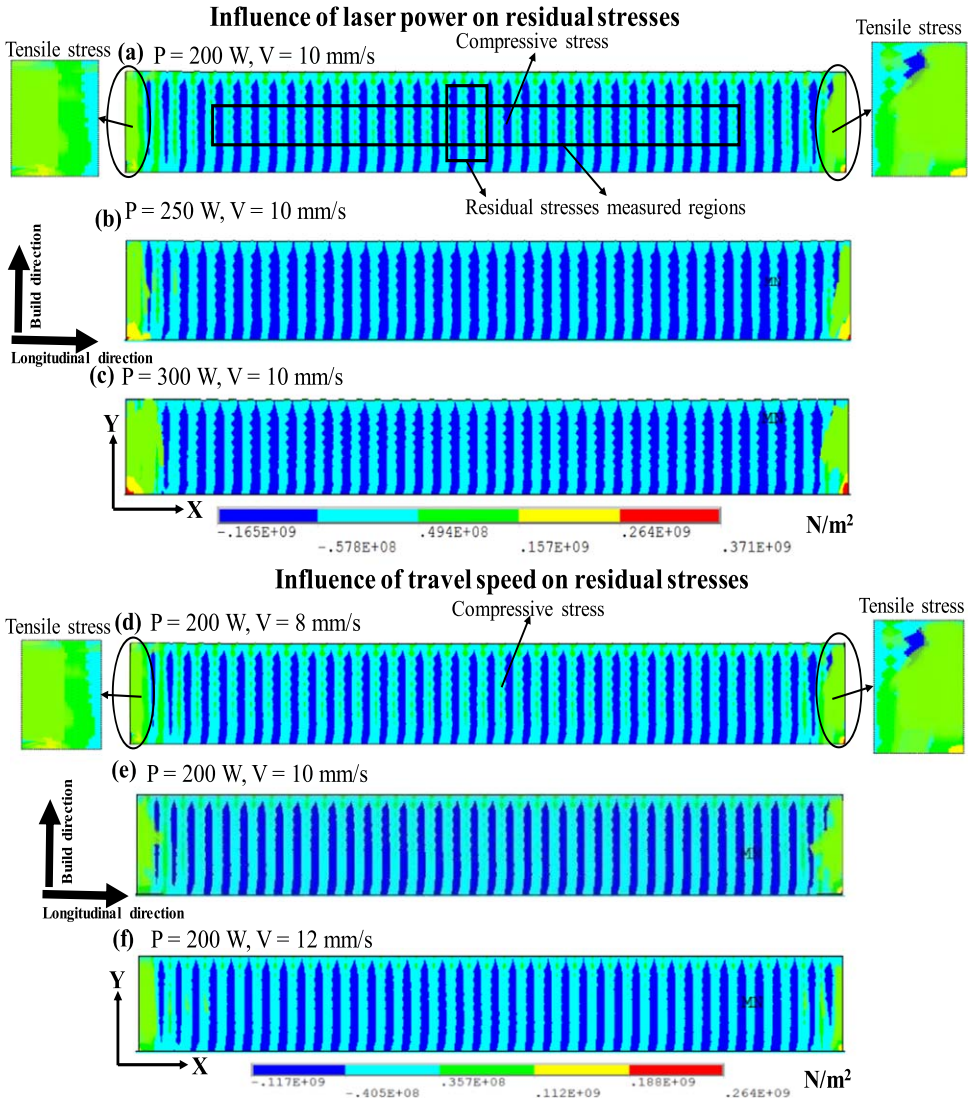

Figure 5. Contour plots showing the influence of laser power and travel speed on the distribution of residual stresses in γ-TiAl thin wall structures build using LENS process.

Table 2. Thermal gradients in the first and last layer of deposition.

Sample number	Thermal gradient (°C/mm) in 1st layer (near to substrate)	Thermal gradient (°C/mm) in 10th layer (top-most layer)
1	6614	11 284
2	6484	10 878
3	6360	10 284
4	7939	13 913
5	7767	13 425
6	7614	12 721
7	9301	16 443
8	9109	15 714
9	8921	14 914

Contours shown in figures 5(d)–(f) were plotted for different travel speeds (V = 8 mm s^{-1}, 10 mm s^{-1}, and 12 mm s^{-1}) at a constant power of 200 W. It can be seen that the trends of stress distribution are analogous to that observed for variation of power at constant travel speed. However, the stress contours for varying travel speed did not show any substantial difference in magnitude. This can be attributed to the fact that the difference in travel speeds considered in this study is only 2 mm s^{-1}.

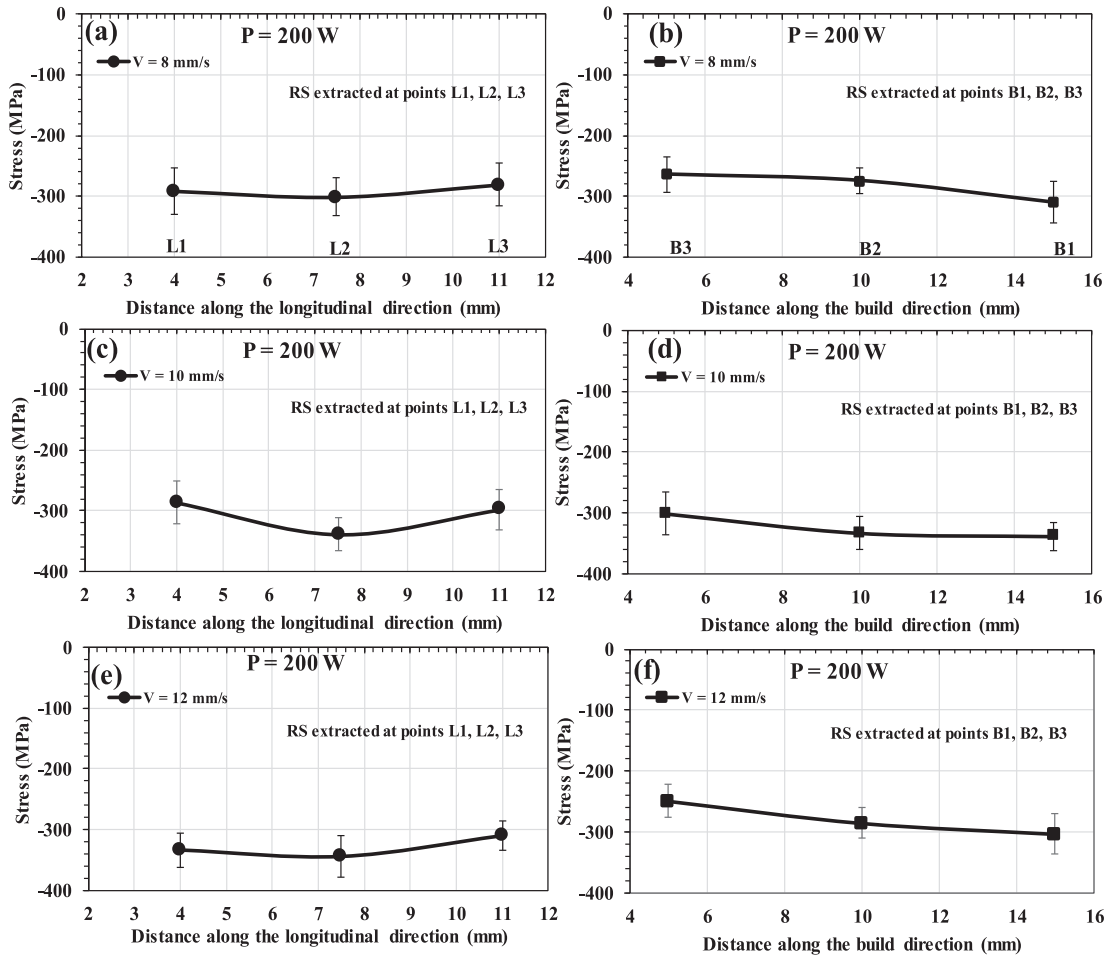

Figure 6. Stress as a function of location along the longitudinal and build directions (a) (b) sample 1, (c) (d) sample 2, (e) (f) sample 3.

During cooling, thermal contraction takes place at the edges as they are free to contract, which is not the case with the material at the centre of the wall. As discussed earlier, the material at the free-edges of the thin-wall is at higher temperatures compared to the material at the centre of the wall. As a result, the hotter free edges start shrinking owing to the reduction in temperature leading to the strain mismatch between the edges and center of the thin wall. Plastic deformation occurs at the free edges as the developed thermal stress exceeds the yield strength of the material. This plastic deformation results in relieving the initially induced compressive stresses at the edges. After completion of cooling, shrinkage at the edges is higher due to solidification and plastic deformation. Thus, tensile stresses are generated at the edges and compressive stresses are generated at the centre region of the thin wall. These results are in agreement with that reported in literature by Rangaswamy *et al* [8] and Wang *et al* [14].

4.2. Measurement of residual stresses by x-ray diffraction technique

The stress distribution measured using x-ray diffraction along longitudinal and build directions for different samples is shown in (figure 6–8). The stresses were measured along the longitudinal direction at a height h = 10 mm (figure 2(b)). In the build direction, the stresses were measured at the centre of the sample (figure 2(c)). In each of the nine thin wall samples, a total of six stress measurements were made (at three points along the horizontal direction and at three points along the vertical direction). Figures 6(a), (c) and (e) show the magnitude of stresses developed along the longitudinal direction for different travel speeds ((V = 8 mm s^{-1}, 10 mm s^{-1}, and 12 mm s^{-1}) at constant power P = 200 W. Similarly, figures 7(a), (c), (e) and 8(a), (c), (e) show the magnitude of stresses developed along the longitudinal direction for different travel speeds at P = 250 W and 300 W respectively. An observation of the above figures reveals that compressive stresses are present in the longitudinal direction in all the samples.

In samples 1–6, (figures 6(a) (c), (e) and 7(a), (c), (e)) measurements indicate that maximum compressive stress is developed at the center (point L2 of figure 2(b)) of the sample. The magnitude of compressive stress decreases with distance from the centre of the sample (points L1 and L3 in figure 2(b)). However, a reverse trend

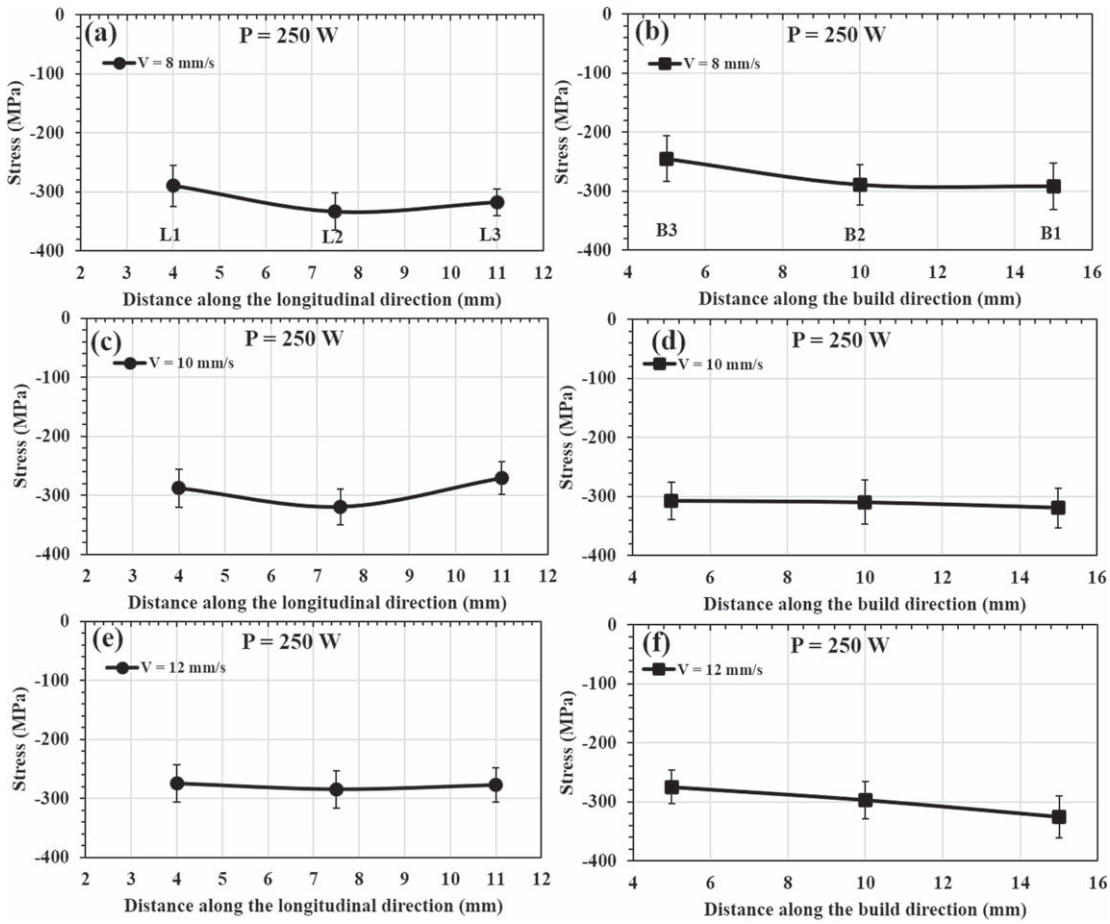

Figure 7. Stress as a function of location along the longitudinal and build directions (a) (b) sample 4, (c) (d) sample 5, (e) (f) sample 6.

to the one observed in samples 1–6 is observed in samples 7 and 8 (figures 8(a) and (c)). That is, maximum compressive stresses were observed at either edge and minimum compressive stress was observed at the centre of the sample. These results highlight the variations in the stresses generated within the thin wall samples. These variations may possibly be attributed to the high surface roughness and material irregularities such as pores/inclusions present at the respective locations where the deviation in trend has been observed in the samples [10].

Figures 6(b), (d) and (f) show the magnitude of stresses developed along the build direction for different travel speeds ((V $=$ 8 mm s^{-1}, 10 mm s^{-1}, and 12 mm s^{-1}) at constant power P $=$ 200 W. Similarly, figures 7(b), (d), (f) and 8(b), (d), (f) show the magnitude of stresses developed along the build direction for different travel speeds at P $=$ 250 W and 300 W respectively. Here again, compressive stresses are present in the build direction in all the samples. In samples 1–6, (figures 6(b) (d), (f) and 7(b), (d), (f)) measurements indicate that magnitude of compressive stresses decreases with increase in the number of layers deposited [8, 22]. On the contrary, samples 7 and 8 (figures 8(b) and (d)) exhibit an opposite trend to that shown by samples 1–6 and 9, along the build direction. As explained earlier, these variations may be attributed to high surface roughness and material irregularities in the samples [10].

In order, to understand the material irregularities, a sample was cold mounted and polished according to metallurgical standards. The optical microscope images of an unetched sample (figures 9(a) and (b)) reveal defects such as pores and inclusions. The pores observed in these optical micrographs are different in size and shape. The presence of defects in the deposited samples could be a possible reason for measurement errors in stresses and also deviations in the plotted trends of stresses.

Figures 10(a) and (b) show the effect of laser power on residual stresses in longitudinal and build directions respectively. From these figures, it is evident that as laser power increases from 200 to 300 W, the magnitude of compressive stress decreases. (Figures 11(a) and (b)) show the effect of travel speed on residual stresses in longitudinal and build directions. The results of figure 11(a) show that compressive stresses increase as the travel speed increases from 8 to 12 mm s^{-1}.

The measured residual stresses in both directions for samples 1–9 are presented in table 3. It can be seen from table 3 that the maximum compressive stresses in the samples are about 49%–79% of yield strength of γ-TiAl

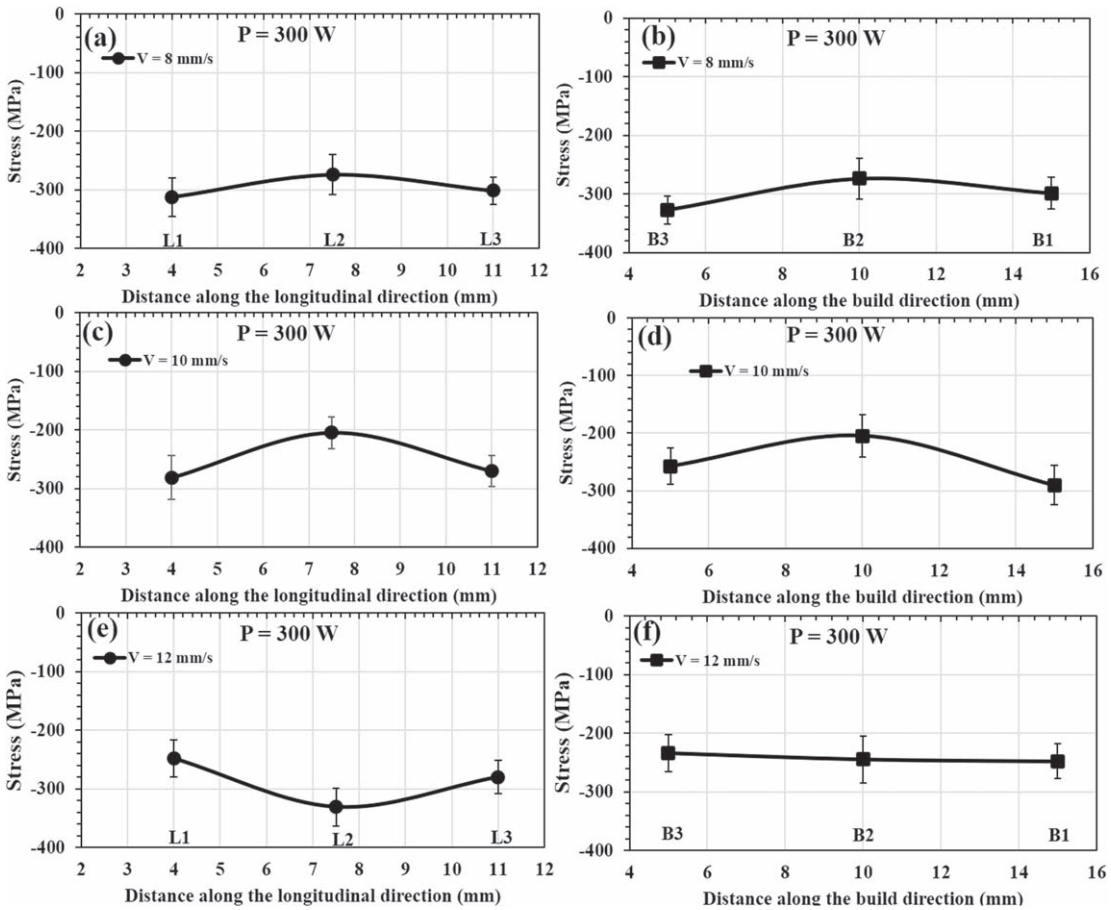

Figure 8. Stress as a function of location along the longitudinal and build directions (a) (b) sample 7, (c) (d) sample 8, (e) (f) sample 9.

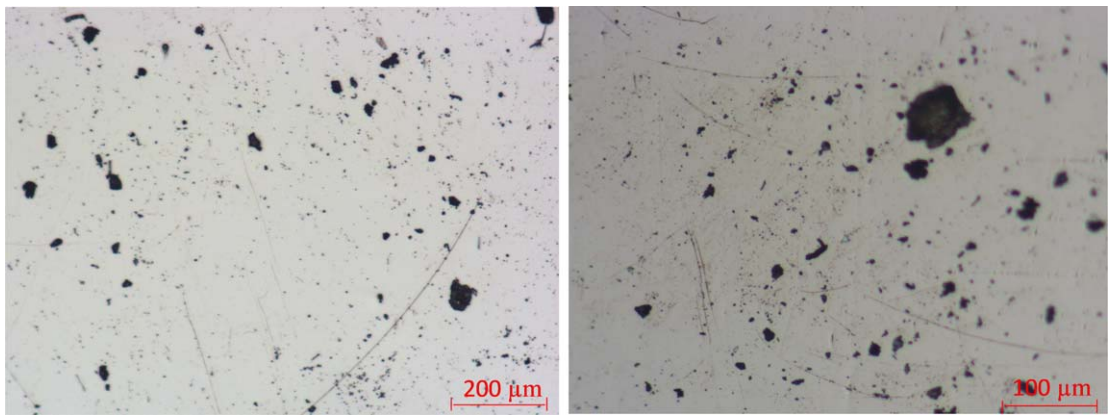

Figure 9. Optical micrographs showing porosity in the γ-TiAl thin wall sample at different magnifications.

alloy [23]. However, trends in experimentally measured stresses reported in this work in both longitudinal and build directions showed good agreement with the existing literature [8, 10]. Further the reliability obtained during the residual stress measurements is in the range of ±40 MPa, which is considered acceptable with respect to the stress measurements made.

4.3. Comparison of modeling and experimental results

Figures 12(a) and (b) present the qualitative comparison between predicted and experimentally measured stresses. Plots show stress distribution in samples 2, 5, and 8 along the longitudinal (figure 12(a)) and build directions (figure 12(b)). Stress values extracted from the finite element models are represented as data points. These points are then curve-fitted using a polynomial function and are denoted by continuous lines. From

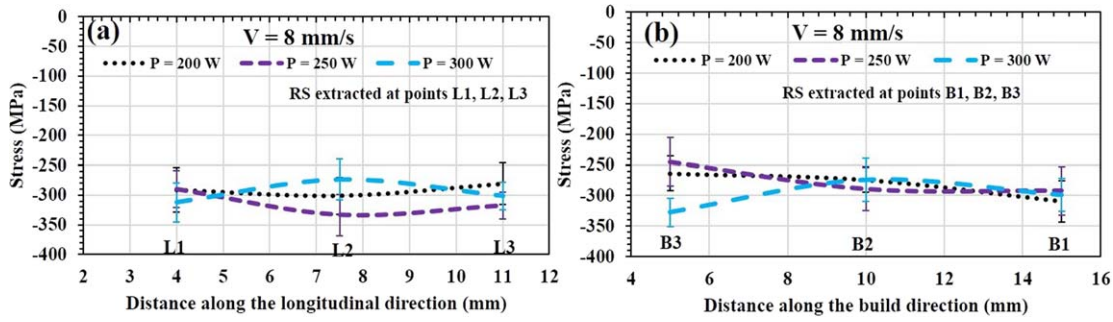

Figure 10. Influence of laser power on stresses in (a) longitudinal direction and (d) build direction.

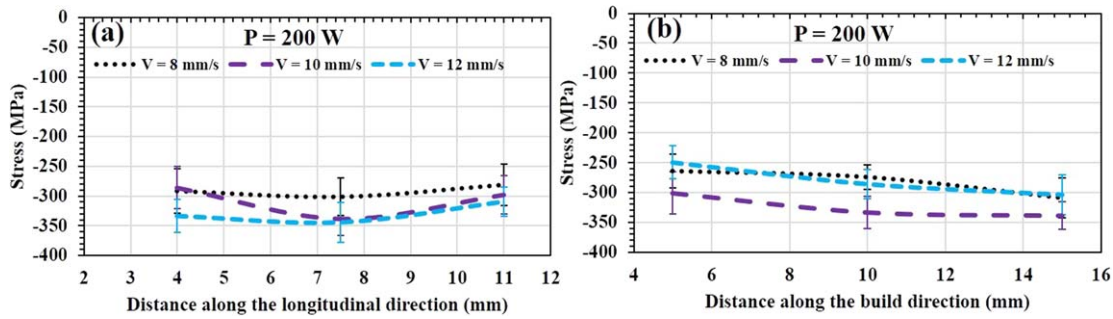

Figure 11. Influence of travel speed on stresses in (a) longitudinal direction and (d) build direction.

Table 3. Measured residual stresses in all thin wall samples along longitudinal and build directions.

Measured Points	L1	L2	L3	B1	B2	B3
Velocity (mm/s)	V = 8	V = 10	V = 12	V = 8	V = 10	V = 12
200 W	−291.4 ± 37.5	−286.1 ± 35.3	−333.7 ± 28.2	−263.9 ± 28.6	−301.2 ± 35.3	−249.5 ± 27.5
	−301.2 ± 31.3	−338.9 ± 27.5	−344.3 ± 33.8	−274.1 ± 20.7	−333.5 ± 27.5	−285.6 ± 24.6
	−281 ± 35.1	−298.1 ± 32.3	−310 ± 24.6	−309 ± 33.8	−338.9 ± 22.8	−303.4 ± 33.5
250 W	−289.5 ± 34.7	−288.1 ± 31.8	−274.8 ± 31.7	−244.9 ± 39	−307.2 ± 27.2	−274.7 ± 28.1
	−333.3 ± 31.2	−319.7 ± 30.7	−285.1 ± 31.9	−289.5 ± 34.7	−309.9 ± 30.7	−296.9 ± 31.7
	−317.3 ± 22.6	−271.1 ± 27.6	−277.5 ± 28.7	−292.2 ± 39.4	−319.7 ± 37.7	−325.6 ± 35.6
300 W	−312.3 ± 32.8	−281.4 ± 37	−248 ± 40	−327.6 ± 23.6	−257.2 ± 31.4	−234.1 ± 31.4
	−273.9 ± 34	−204.7 ± 27	−331 ± 38	−273.9 ± 35.1	−204.7 ± 37.3	−244.7 ± 40
	−301.6 ± 23.6	−270.1 ± 26.4	−279.7 ± 36.7	−299 ± 27.3	−290.4 ± 34	−248 ± 29.5

figures 12(a) and (b), it can be seen that the predicted residual stress distribution follows a similar trend as the experimentally measured ones. Figure 12(a) shows the stress distribution along the longitudinal direction of the thin wall. Results show tensile stresses at the edges and compressive stresses in the core. This is due to imposed thermal gradients and plastic deformation. Further, a comparison of the trends in stresses obtained from numerical models and experimentally measured ones showed a good agreement.

Figure 12(b) shows the predicted and measured residual stresses along the build direction of samples. Numerical modelling predictions of stress distribution in the build direction reveal tensile stresses in the topmost layer of the wall, and compressive stresses in the rest of the thin-wall. It was found that there is a good agreement between the predicted and experimental results. The discrepancy between the predicted and measured stress results can be attributed to the assumptions (neglection of convection, radiation and Marangoni effect etc,) that were made in the numerical models. Further, the predicted stress distribution trends are in good agreement with those reported in literature [1014, 24].

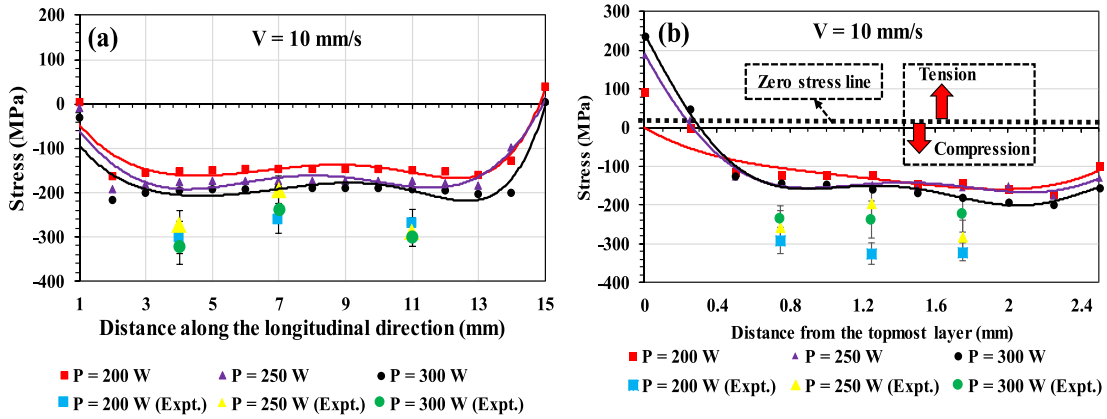

Figure 12. Comparison of numerical and experimental stress along (a) longitudinal direction and (b) build direction for different laser powers.

5. Conclusions

The state and magnitude of residual stress distribution in laser metal deposited γ-TiAl thin wall structures were predicted using 3D transient thermomechanical analysis and also measured experimentally using x-ray diffraction technique. The following are the conclusions of the present work:

- Thermal gradients increase with the addition of each deposited layer, i.e., from the first to the last layer.
- The state and magnitude of residual stress distribution in the thin walls can be attributed to the transient thermal gradients encountered during deposition.
- In the build direction, compressive stress decreases with increase in the number of deposited layers.
- Under the present experimental conditions, changes in laser power and travel speed did not show any substantial effect on the stress distribution.
- The trends in predicted and measured residual stresses are in good agreement with each other in both longitudinal and build directions.

Acknowledgments

Gratitude is hereby expressed to Mr V Srikant, Sci 'D' and Dr S S Panwar, Sci 'F' of the Material Development Division, Defense Research & Development Laboratory (DRDL), Kanchanbagh, Hyderabad, India, for giving permission to measure residual stresses using x-ray diffraction facility in their lab.

ORCID iDs

Mallikarjuna Balichakra https://orcid.org/0000-0001-5598-0219
Srikanth Bontha https://orcid.org/0000-0002-8803-6774

References

[1] Appel F and Paul D H 2011 *Gamma Titanium Aluminide Alloys: Science and Technology* 12 (Weinheim, Germany: Wiley-VCH Verlag GmbH & Co. KGaA) (https://doi.org/10.1002/9783527636204)
[2] Bewlay B P, Nag S, Suzuki A and Weimer M J 2016 TiAl alloys in commercial aircraft engines *Mater. High Temp.* **33** 549–59
[3] Kothari K, Radhakrishnan R and Wereley N M 2012 Advances in gamma titanium aluminides and their manufacturing techniques *Prog. Aerosp. Sci.* **55** 1–16
[4] Zhang X D, Brice C, Mahaffey D W, Zhang H, Schwendner K, Evans D J and Fraser H L 2001 Characterization of laser-deposited TiAl alloys *Scr. Mater.* **44** 2419–24
[5] Balla V K, Das M, Mohammad A and Al-Ahmari A M 2016 Additive manufacturing of γ-TiAl: processing, microstructure, and properties *Adv. Eng. Mater.* **18** 1–8
[6] Saboori A, Gallo D, Biamino S, Fino P and Lombardi M 2017 An overview of additive manufacturing of titanium components by directed energy deposition: microstructure and mechanical properties *Appl. Sci.* **7** 883
[7] Withers P J J and Bhadeshia H K D H 2001 Residual stress:I. Measurement techniques *Mater. Sci. Technol.* **17** 355–65

[8] Rangaswamy P, Griffith M L, Prime M B, Holden T M, Rogge R B, Edwards J M and Sebring R J 2005 Residual stresses in LENS ® components using neutron diffraction and contour method *Mater. Sci. Eng.* A **399** 72–83
[9] Moat R J, Pinkerton A J, Hughes D J, Li L, Withers P J and Preuss M 2007 Stress distributions in multilayer laser deposited Waspaloy parts measured using neutron diffraction *26th Int. Congr. Appl. Lasers Electro-optics* (https://doi.org/10.2351/1.5060984)
[10] Pratt P, Felicelli S D, Wang L and Hubbard C R 2008 Residual stress measurement of laser-engineered net shaping AISI 410 thin plates using neutron diffraction *Metall. Mater. Trans.* A **39** 3155–63
[11] Long R-S, Liu W-J and Xing Fei W H 2007 Numerical simulation of the thermal behavior during laser metal deposition shaping technology *Trans. Nonferrous Met. Soc. China* **380–384** 4327–31
[12] Moat R J, Pinkerton A J, Li L, Withers P J and Preuss M 2010 Residual stresses in laser direct metal deposited Waspaloy *Mater. Sci. Eng. A* **528** 2288–98
[13] Vogel M, Khan M, Ibarra-Medina J, Pinkerton A J, Group M, Street S and Kingdom U 2012 A verified model of transient and residual stresses in laser direct metal deposition *Int. Congr. Appl. Lasers Electro-Optics* **89** 89–96
[14] Wang L, Felicelli S D and Pratt P 2008 Residual stresses in LENS-deposited AISI 410 stainless steel plates *Mater. Sci. Eng.* A **496** 234–41
[15] Sung S Y and Kim Y J 2006 Modeling of titanium aluminides turbo-charger casting *Intermetallics* **15** 468–74
[16] Yan L, Li W, Chen X, Zhang Y, Newkirk J, Liou F and Dietrich D 2016 Simulation of cooling rate effects on Ti-48Al-2Cr-2Nb crack formation in direct laser deposition *JOM Proc. 27th Annu. Int. Solid Free. Fabr. Symp. Addit. Manuf. Conf.* **69** 586–91
[17] Balichakra M, Bontha S, Krishna P and Balla V K 2019 Laser surface melting of γ-TiAl alloy an experimental and numerical modeling study *Mater. Res. Express* **6** 046543
[18] Fallah V, Alimardani M, Corbin S F and Khajepour A 2011 Temporal development of melt-pool morphology and clad geometry in laser powder deposition *Comput. Mater. Sci.* **50** 2124–34
[19] Heigel J C, Michaleris P and Reutzel E W 2015 Thermo-mechanical model development and validation of directed energy deposition additive manufacturing of Ti–6Al–4V *Addit. Manuf.* **5** 9–19
[20] Denlinger E R, Irwin J and Michaleris P 2014 Thermomechanical modeling of additive manufacturing large parts *J. Manuf. Sci. Eng.* **136** 061007
[21] Lavanya S, Mahadevan S and Mukhopadhyay C K 2019 Correlation of tensile deformation-induced strain in HSLA steel with residual stress distribution *J. Mater. Eng. Perform.* **28** 1103–11
[22] Sammons P M, Bristow D A and Landers R G 2013 Height dependent laser metal deposition process modeling *J. Manuf. Sci. Eng.* **135** 054501
[23] Kim Y W 1989 Intermetallic alloys based on gamma titanium aluminide *J. Mater. Sci. Eng.* **41** 24–30
[24] Martina F, Roy M J, Szost B A, Terzi S, Colegrove P A, Williams S W, Withers P J, Meyer J and Hofmann M 2016 Residual stress of as-deposited and rolled wire+arc additive manufacturing Ti–6Al–4V components *Mater. Sci. Technol.* **32** 1439–48